Features of the Observed Annual Ocean–Atmosphere Flux Variability on the West Florida Shelf

JYOTIKA I. VIRMANI AND ROBERT H. WEISBERG

College of Marine Science, University of South Florida, St. Petersburg, Florida

(Manuscript received 1 November 2001, in final form 7 March 2002)

ABSTRACT

The annual cycle of sea surface temperature and ocean–atmosphere fluxes on the west Florida shelf is described using in situ measurements and climatology. Seasonal reversals in water temperature tendency occur when the net surface heat flux changes sign in boreal spring and fall. Synoptic-scale variability is also important. Momentum and heat flux variations result in successive water column stratification and destratification events, particularly at shallower depths during spring. Fall is characterized by destratification of the water column and a series of steplike decreases in the temperature. These are in response to both tropical storms and extratropical fronts. Tropical storms are responsible for the largest momentum fluxes, but not necessarily for the largest surface heat fluxes. A one-dimensional analysis of the temperature equation suggests that surface heat flux is primarily responsible for the spring and fall seasonal ocean temperature changes, but that synoptic-scale variability is also controlled by the ocean circulation dynamics. During summer, the situation is reversed and the major influence on water temperature is ocean dynamics, with the heat flux contributing to the synoptic-scale variability. There is also evidence of interannual variability: the wintertime temperatures get increasingly colder from 1998 to 2000, and the greatest stratification and coldest subsurface temperatures occur in 1998. NCEP–NCAR reanalysis fields do not reproduce the high spatial flux variability observed in situ or with satellite measurements. Reconciling these differences and their impacts on the climate variability of this region provides challenges to coupled ocean–atmosphere models and their supporting observing systems.

1. Introduction

Sea surface temperature (SST) within the Gulf of Mexico (hereafter Gulf) shows considerable spatial and temporal variability. Some of this variability is due to ocean dynamics associated with coastal upwelling and the Loop Current, but an equally important amount is due to local ocean–atmosphere fluxes. In all but the summer months the coastal regions of the Gulf are generally cooler than the midbasin, where Loop Current intrusion provides a relatively uniform delivery of warm water. These temperature contrasts produce basinwide SST gradients and variations in the surface heat, moisture, and momentum fluxes that influence the climate of the Gulf and surrounding landmasses. Understanding causes of SST variability in this region is important because the Gulf is a major source of moisture flux to the U.S. heartland (Rasmusson 1967).

The west Florida continental shelf (WFS) occupies the eastern side of the Gulf. Except for the Florida Panhandle in the north where the shelf narrows to a minimum width at DeSoto Canyon, the WFS is broad and gently sloping. It supports a highly diverse and productive ecosystem, and it has a major influence on the climate of the surrounding landmasses. The coastline and isobath geometries greatly impact the WFS circulation and the heat and moisture fluxes of this region. Observation and modeling efforts are under way to investigate the interactions between the WFS and the climate of the Gulf. To date, most observational studies have concentrated on the WFS ocean circulation (e.g., Niiler 1976; Williams et al. 1977; Weisberg et al. 1996), the influence of the Loop Current (e.g., Huh et al. 1981; Sturges and Leben 2000), its tides (e.g., Koblinsky 1981; Weatherly and Thistle 1997; He and Weisberg 2002a), the effects of winds (e.g. Fernandez-Partagas and Mooers 1975; Mitchum and Sturges 1982; Marmorino 1982; Cragg et al. 1983; Clarke and Brink 1985; Mitchum and Clarke 1986; Weisberg et al. 2001), and the impact of tropical storms on the WFS ocean mixed layer (Price et al. 1978). Less attention has been given to the effect of the annual cycle of heat fluxes on the WFS and its adjacent landmass.

This paper describes the annual cycle of observed atmospheric fluxes and ocean temperatures at three locations on the WFS. The following section gives an overview of the annual cycle over the Gulf region, and previous observational and modeling work over the

Corresponding author address: Jyotika I. Virmani, College of Marine Science, University of South Florida, 140 Seventh Ave. S., St. Petersburg, FL 33701.
E-mail: jvirmani@marine.usf.edu

WFS. Details of the observations used in this work are given in section 3. A description and discussion of the annual cycle of observed ocean temperatures and associated air–sea fluxes for this region of the WFS is in section 4. Finally, section 5 contains a summary of the salient features.

2. Background

In broad terms, the annual cycle of SST in the Gulf is fairly well defined. The Loop Current advects relatively warm Caribbean waters into the eastern Gulf yearround (Fig. 1). Combined with local heating, SST tends to be uniformly warm in boreal summer, and when SST exceeds 28.5°C the Gulf is part of the Western Hemisphere warm pool (WHWP; Weisberg 1996; Wang and Enfield 2001). However, seasonal upwelling often results in cold water on the shallow Campeche Banks, along the Mexican coast, along the northern Gulf coast east of the Mississippi River delta, and on the WFS. Therefore the coastal waters tend to be much cooler—with as much as a 10°C difference in SST between the Loop Current and the coastal waters, particularly during the winter and spring seasons. These temperature differences produce basinwide SST gradients and variations in the surface heat, moisture, and momentum fluxes that influence the climate of the Gulf of Mexico and its surroundings.

There are also seasonal atmospheric variations that affect the climate of this region (Fig. 1). In boreal winter, a zonal ridge of high pressure extends westward from the Atlantic across the southern United States and the northern Gulf. In boreal summer, the Bermuda high is better defined, with the high pressure system confined to the western Atlantic only. This pressure system is integral in driving the wind field across the Gulf of Mexico and the United States.

The National Centers for Environmental Prediction (NCEP) climatological heat flux components averaged over the Gulf (Fig. 2) show an annual cycle, with heating of Gulf waters from approximately March to September and cooling at other times. The largest annual variation is in the net shortwave radiation (SW), which peaks in May. There is also a large annual cycle in the latent heat flux with a range of almost 100 W m^{-2}, and a maximum during winter. With the addition of the net longwave radiation (LW) and sensible heat flux, the annual cycle in the net heat flux is obtained and varies from about 80 W m^{-2} during the summer to -150 W m^{-2} during the winter (positive and negative values being fluxes into and out of the ocean, respectively). Geographically, the largest annual variability in the latent heat flux climatology occurs east of the Mississippi River delta in the winter and is associated with the warm waters of the Loop Current. Using the Da Silva et al. (1994) data, Wang and Enfield (2001) reported a similar annual cycle of fluxes for the entire WHWP region. Averaging the NCEP flux climatology components over the same region for direct comparison with the Da Silva climatology shows that although the overall features of the annual cycle are the same between the two climatologies, there is a discrepancy in the magnitudes. From Wang and Enfield (2001), the maximum net SW radiation in the Da Silva data is ~30 W m^{-2} greater than NCEP during boreal spring and summer. The next largest component, the latent heat flux has ~10 W m^{-2} larger loss in NCEP than in the Da Silva data. The sensible heat flux and net LW radiation losses are also slightly larger in the NCEP climatologies. Therefore, the net heat flux averaged over the WHWP during the spring and summer from the NCEP climatology is ~60 W m^{-2} less than that produced by the Da Silva climatology. This is an example of the large discrepancies that currently exist between different climatologies.

Previous observations on the WFS show that the ocean circulation is affected by a combination of factors. The Loop Current intrudes into the northern Gulf (e.g., Huh et al. 1981), shedding eddies every 6–17 months (e.g., Vukovich 1988; Sturges 1994; Sturges and Leben 2000) and inducing low-frequency variations on the outer portions of the WFS (Niiler 1976; Maul 1977; Meyers et al. 2001). On the shelf, seasonal changes in the circulation have been detected by two sets of in situ measurements: drifters (Williams et al. 1977) and moored buoys (Weisberg et al. 1996). These measurements suggest that the strongest alongshore midshelf currents occur during the transition seasons, such that during spring they are southeastward and in fall they are northwestward. Synoptic-scale variability on the mid- and inner shelf regions can result from atmospheric forcing (e.g., Blaha and Sturges 1981; Mitchum and Sturges 1982; Marmorino 1982). Satellite data show that SST can respond rapidly to synoptic-scale atmospheric forcing, in the form of well-developed upwelling-induced cold tongues (e.g., Weisberg et al. 2000). The trailing edge of subsynoptic wintertime frontal systems are also generally upwelling favorable (Fernandez-Partagas and Mooers 1975). On smaller timescales, diurnal variability plays an important part on the WFS: tidal observations have shown that the WFS is dominated by mixed semidiurnal and diurnal tides (e.g., Koblinksy 1981; Marmorino 1983; Weatherly and Thistle 1997; He and Weisberg 2002a). One of the few studies of ocean–atmosphere interactions on the WFS concerned the impact of tropical storms on the ocean mixed layer and air–sea heat exchange. Price et al. (1978) used observations and a model for this investigation and found that entrainment at the base of the mixed layer was the primary mechanism for observed deepening of the mixed layer and ocean cooling.

Model studies provide insights on the seasonal WFS circulation. Using an adaptation of the Princeton Ocean Model (POM) forced by the Hellerman and Rosenstein (1983) climatological wind fields, Yang and Weisberg (1999) diagnosed the monthly mean circulation patterns of the WFS. Climatological winds alone were found to

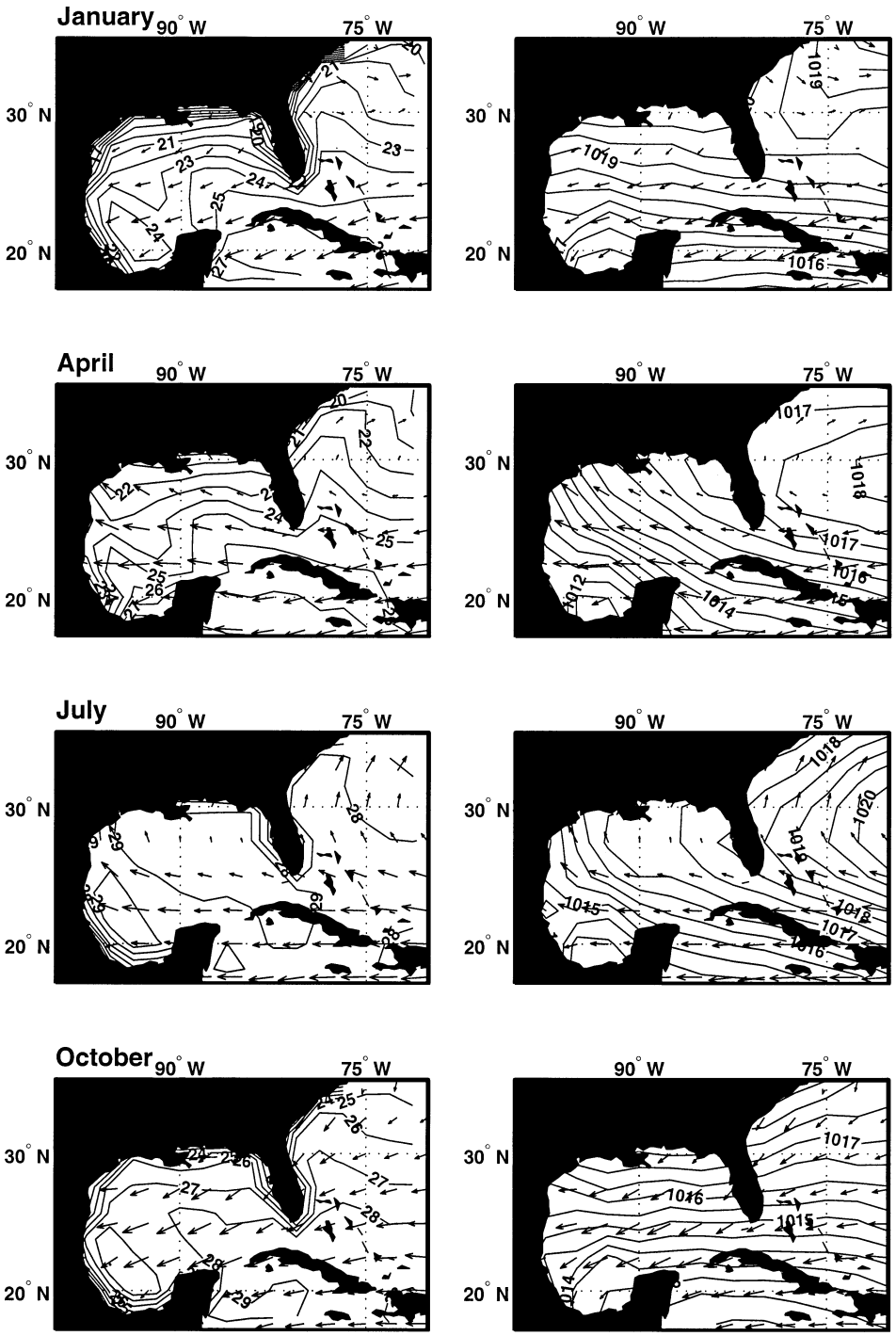

FIG. 1. NCEP climatological wind field (arrows) overlaying (left) the skin temperature and (right) sea level pressure over the western Atlantic Ocean and the Gulf of Mexico for (top) Jan, (second) Apr, (third) Jul, and (bottom) Oct. Contour intervals for temperature are 1°C. Contour intervals for pressure are 0.5 mb.

be insufficient, suggesting that heat flux and baroclinicity must also be important. He and Weisberg (2002b) applied the POM using NCEP–National Center for Atmospheric Research (NCAR) reanalysis winds and heat flux as inputs. Because of low spatial resolution in the NCEP reanalysis grid, a heat flux relaxation to SST was required to capture the WFS cold tongue. With the flux correction, the model baroclinic field accounted for the

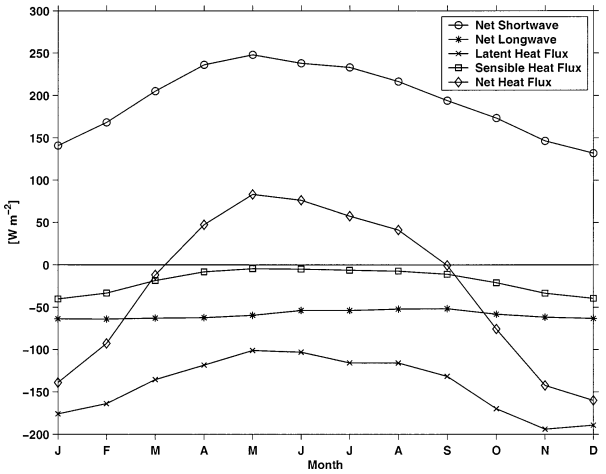

FIG. 2. NCEP climatological heat flux components averaged over the Gulf of Mexico.

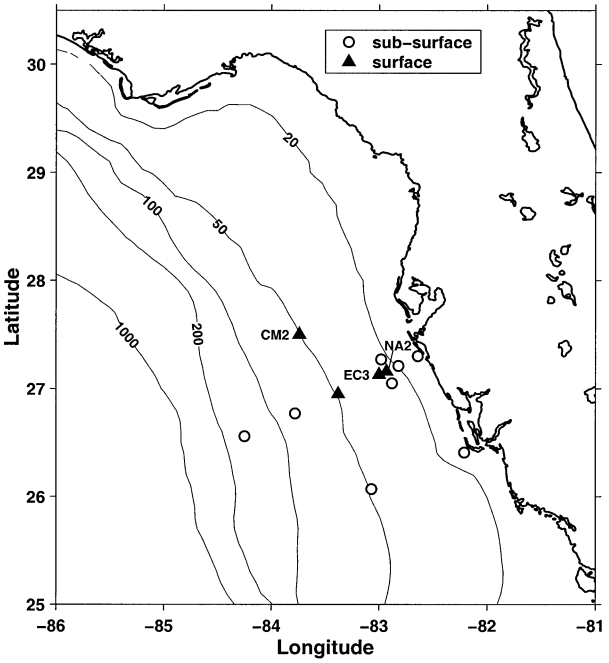

FIG. 3. The University of South Florida's array of subsurface and surface moorings on the west Florida shelf. The data in this study are from the moorings marked by solid triangles and labeled.

spring season circulation. As an essential contributor to understanding the seasonal circulation on the WFS, adequate surface heat (and momentum) flux fields are required, necessitating improvements to both models and in situ measurements for this region.

3. Observations

Since 1998, and in contribution to multidisciplinary studies, University of South Florida personnel have maintained an array of up to 12 buoys on the WFS (Fig. 3). In addition to measuring currents, temperature, and salinity, four buoys were equipped with meteorological sensors for air temperature, relative humidity, precipitation, wind speed and direction, and barometric pressure. Two moorings also measured downward longwave and shortwave radiation. The surface meteorological measurements were made by a combination of Coastal Climate Weatherpaks and Woods Hole Oceanographic Institution (WHOI) designed improved meteorology (IMET) or air sea interaction–meteorology (ASIMET) systems.

Data from the moorings CM2, EC3, and NA2 (Fig. 3) are used. These contain the most complete sets of data (both subsurface temperatures and surface meteorological measurements, Figs. 4–6) from June 1998 to March 2001. NA2 was 37 km offshore at the 25-m isobath. EC3, approximately 9 km from NA2, was 46 km offshore near the 30-m isobath. CM2 was the farthest offshore mooring to be considered here, and was 102 km offshore in water depth of about 50 m.

The water salinity and temperature data, measured using Sea-Bird Electronics SeaCATs and MicroCATs, and TSKA WaDaRs were sampled every 10 min. The Weatherpak collected 1-s samples and returned a 15-min average, and the IMET/ASIMET samples were averaged over a 1-min duration every 20 min. Hourly averages of these data were used to make the surface heat flux calculations. Most of the data analysis and description of seasons and events are based on these hourly averages. Smoothing using the 36-h low-pass Butterworth filter was used to identify features within the entire time series. The analysis of the one-dimensional temperature equation required further data processing. Using the vertically integrated temperature, extrapolated to the depth of the mooring, dT/dt was calculated using a fast Fourier transform, and then low-pass filtered as above.

Before using the data to make any calculations, some measurement error mitigation was done by comparing data from corresponding instruments on the NA2 and EC3 moorings. An example is given in Fig. 7, which shows the downward LW, SW, and SST measurements at NA2 (IMET) and EC3 (Weatherpak) during May 2000. Note that SST is the shallowest measurement of temperature at a depth of 1 m, and not the skin temperature. The SST and downward SW compare favorably; however, there is an offset in the downward LW of about 50 W m^{-2}. At first glance, it is not obvious which sensor is correct, because both values fall within previously observed ranges (Weller and Anderson 1996; Josey et al. 1997). Parameterizations of downward LW radiation (e.g., Berliand and Berliand 1952; Anderson 1952; Clark et al. 1974; Bunker 1976) were used with observed SST, air temperature, and barometric pressure to calculate the expected downward LW radiation. These showed that regardless of the amount of cloud cover, the values of calculated downward LW agree more closely with those measured at EC3. It was since de-

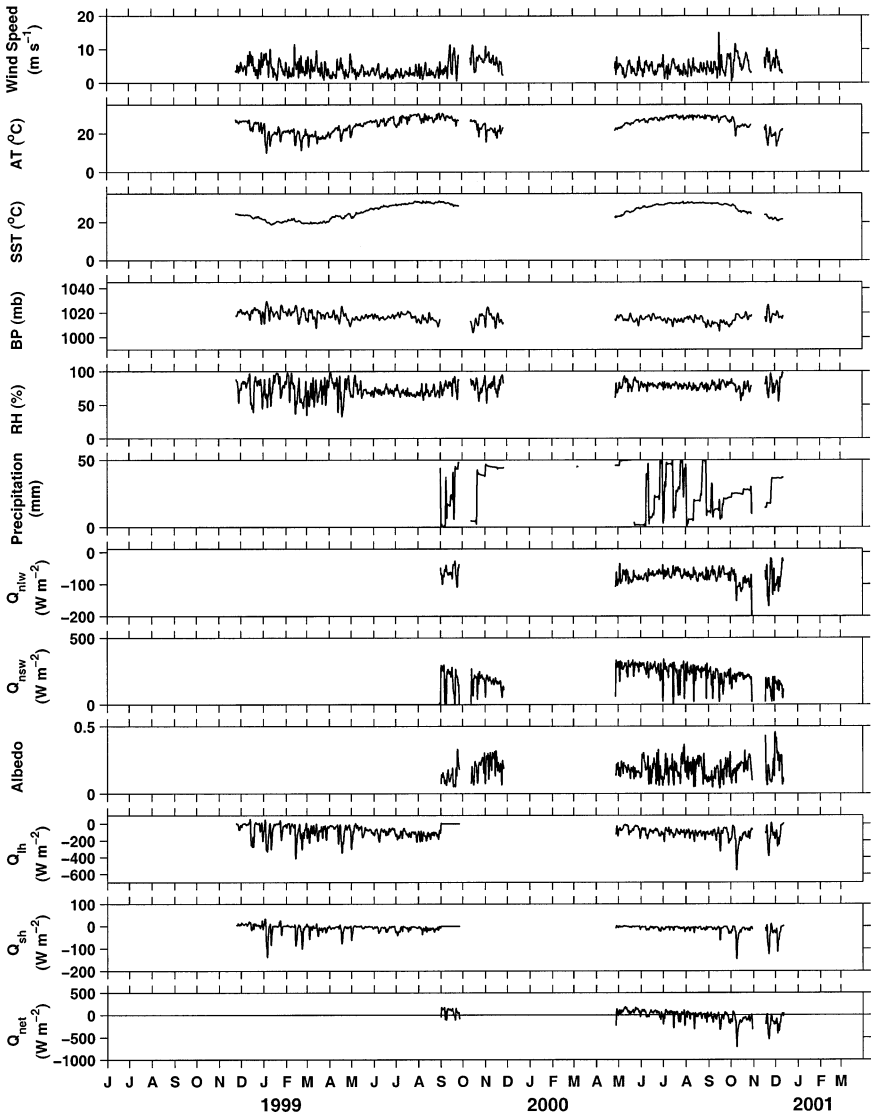

FIG. 4. Low-pass (36-h Butterworth) filtered meteorological time series and calculated heat fluxes from NA2 between Jun 1998 and Mar 2001.

termined that the NA2 IMET LW sensor from May to December 2000 was incorrectly calibrated and was rectified for subsequent deployments. A discrepancy was also found in the pressure sensors, with readings at EC3 being about 6 mb higher than those at NA2 for 2000. It is currently unknown which pressure sensor is correct. However, as this results in a net heat flux difference of less than 1 W m^{-2} it is not a major source of error. Relative humidity sensors also showed an offset of about 7%, with NA2 being higher than EC3. Comparisons with data from CM2 (Weatherpak) showed relative humidity values that were closer to EC3. We believe that the NA2 RH sensor calibration is correct, suggesting that there may be calibration problems with the Weatherpak RH sensors. A discrepancy of 7% in RH is not unheard of, and was also noted during the Tropical Ocean Global Atmosphere Coupled Ocean–Atmosphere Response Experiment (TOGA COARE; Weller and Anderson 1996). This resulted in errors of up to 30 W m^{-2}, and the source of this is being investigated. Hourly averaged values were used to calculate the surface heat and momentum fluxes using the MATLAB air–sea fluxes toolbox, which uses bulk parameterizations of surface fluxes.

4. Description and discussion

As expected in the Northern Hemisphere, the temperatures in the water column at all locations showed warming during spring and early summer, peaking in August, and cooling during fall, usually reaching a minimum in February (Fig. 8). There is an approximate 90°

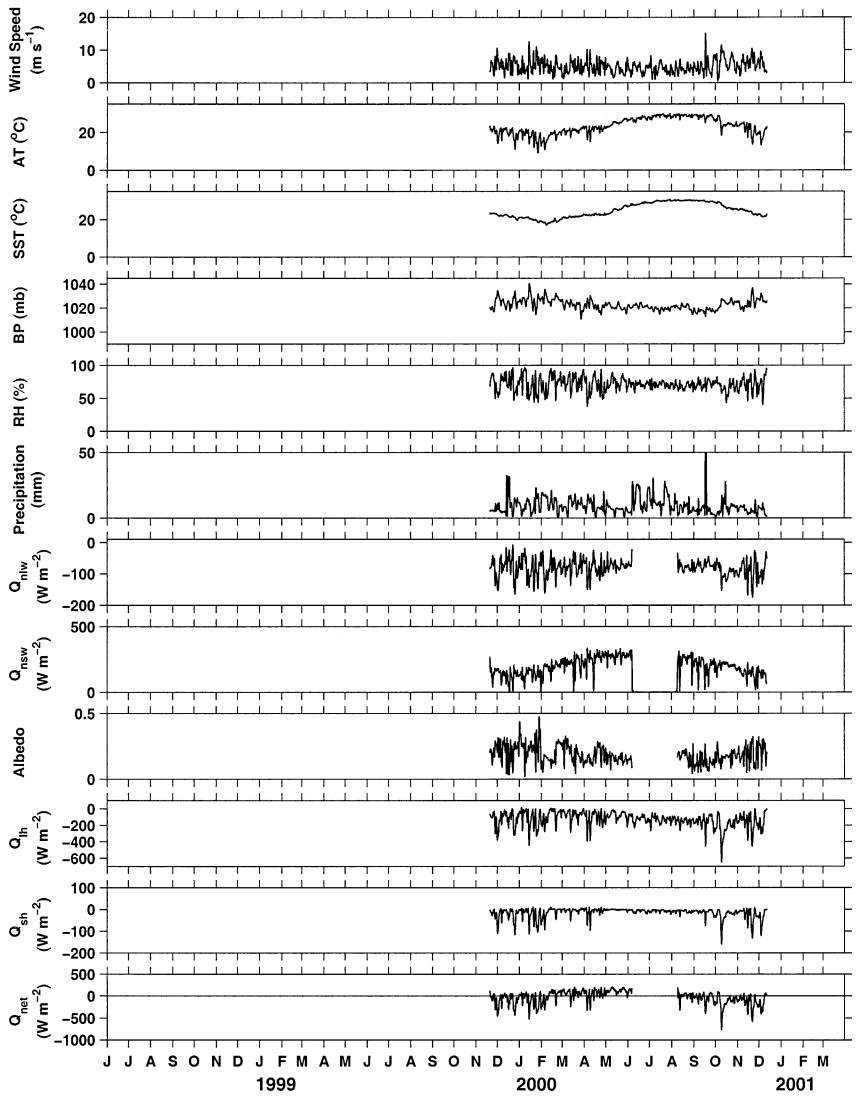

FIG. 5. Same as Fig. 4, but from EC3.

phase shift between the annual cycles of temperature and net heat flux, with heat flux leading temperature; that is, waters begin their seasonal warming or cooling when the net surface heat flux switches sign in the spring and fall and the largest rate of change of temperature occurs when the net surface heat flux is largest. During the spring transition season, temperatures are increasing and the heat gain to the ocean is greatest. Conversely, during the fall transition season, decreasing temperatures correspond to a time of maximum heat loss from the ocean.

During spring and early summer (February–July), in addition to gradually increasing water temperatures, the subsurface temperature profile shows considerable stratification. At NA2 and EC3, variations in stratification occur at synoptic timescales (Fig. 9a). Decreases in wind stress and increases in surface heat flux cause increases in stratification. Decreased wind stress leads to decreased turbulent mixing, and increased heat (buoyancy) flux leads to increased water column stability. Ocean current data collected at NA2 during this time period (not shown) shows that coastal upwelling, in response to increased wind stress, is coincident with all periods of stratification during May and June, however, in July stratification occurs without upwelling. Conversely, downwelling results predominantly in destratification, however, there are times when destratification occurs without any associated downwelling. This shows the complicated interplay between ocean dynamics and surface heat flux in determining the temperature of the water column. Such synoptic-scale variability is not as evident at the farthest offshore CM2 site where the stratification is larger, requiring proportionately larger flux variations to affect change.

To determine the relative importance of the surface heat flux and ocean dynamics in controlling SST, we

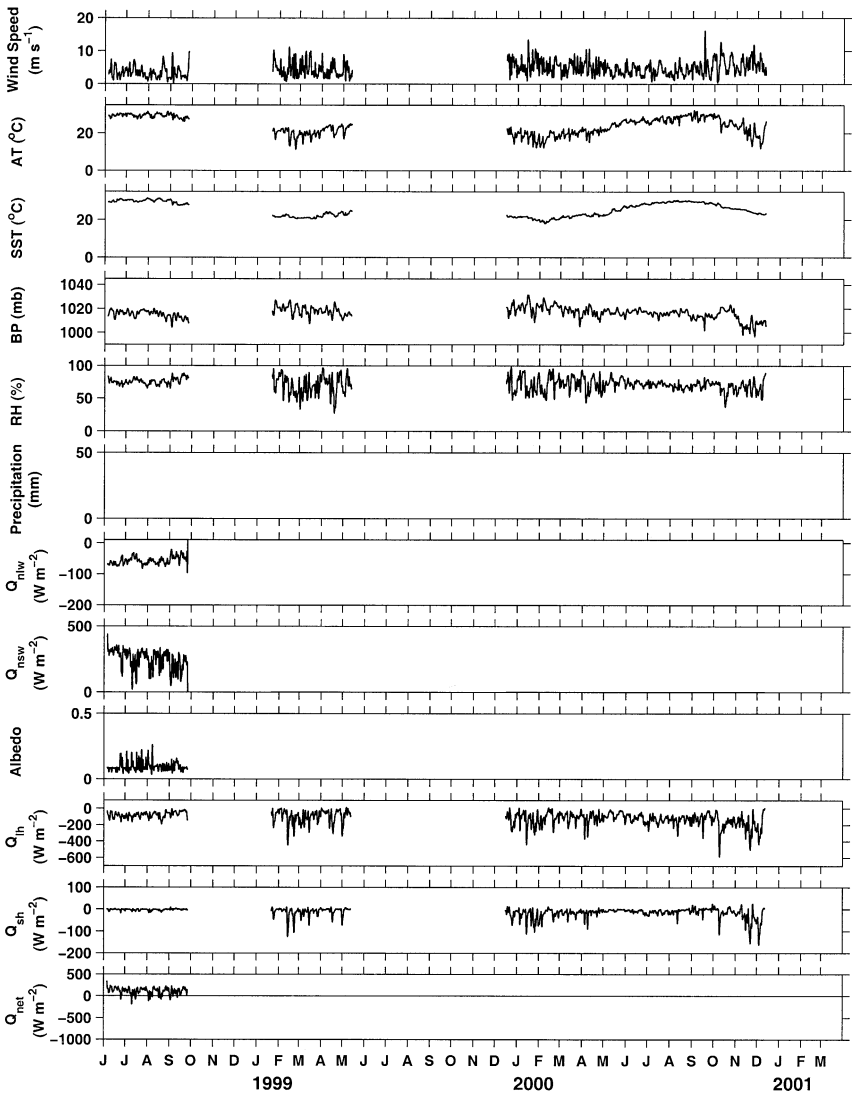

FIG. 6. Same as Fig. 4, but from CM2.

analyzed the one-dimensional depth-averaged temperature equation using the corrected data from NA2:

$$\frac{\partial T}{\partial t} = \frac{Q_{\text{net}}}{c_p \rho H}, \tag{1}$$

where T is the vertically integrated temperature, c_p is the heat capacity of seawater (3998 J kg^{-1} K^{-1}), ρ is the density of seawater (1023.34 kg m^{-3}), H is the water depth, and Q_{net} is the net surface heat flux from

$$Q_{\text{net}} = Q_{\text{sw}} + Q_{\text{lw}} - Q_{\text{lh}} - Q_{\text{sh}} - Q_{\text{pen}}, \tag{2}$$

where Q_{sw} is the net shortwave radiation, Q_{lw} is the net longwave radiation, Q_{lh} is the latent heat flux, Q_{sh} is the sensible heat flux, and Q_{pen} is the penetrative radiation over twice the depth of the water column. The assumption made is that no radiation is absorbed at the coastal ocean floor, instead it is entirely reflected and therefore contributes to the heat loss from the ocean. An estimate of Q_{pen}, with maximum values of 31 W m^{-2}, at NA2 was obtained using the Paulson and Simpson (1977) parameterization for type-1A water (Jerlov 1968). The residual, obtained by subtracting the right side of (1) from the left, accounts for the three-dimensional effects of ocean circulation dynamics on dT/dt, that is, advection, and any remaining errors.

The change in the vertically integrated water temperature at NA2 during May–July is 6.92°C, of which 3.28°C (47.5%) results from surface heat flux, and 3.63°C (52.5%) results from ocean dynamics. The currents along the WFS during this time are predominantly northwestward, advecting warmer water from the south, so ocean dynamics are marginally more important in affecting temperature change over this 3-month period than the surface heat flux. However, on a month-by-month basis, the relative importance of these two factors changes because this period covers the transition of the

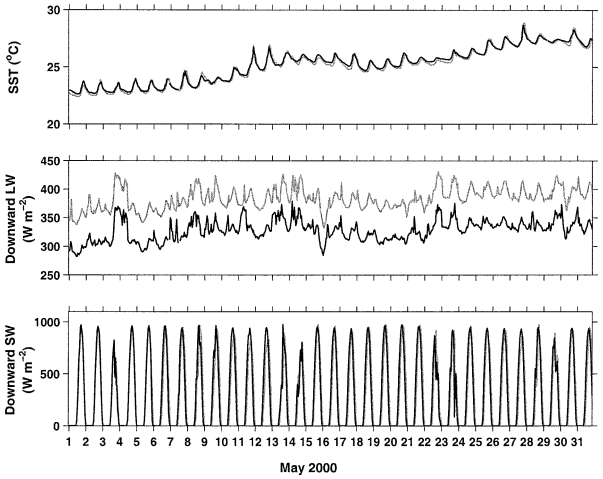

FIG. 7. Comparison of meteorological measurements from NA2 (dark line) and EC3 (light line) during May 2000. (top) SST, (middle) downward longwave radiation, and (bottom) downward shortwave radiation.

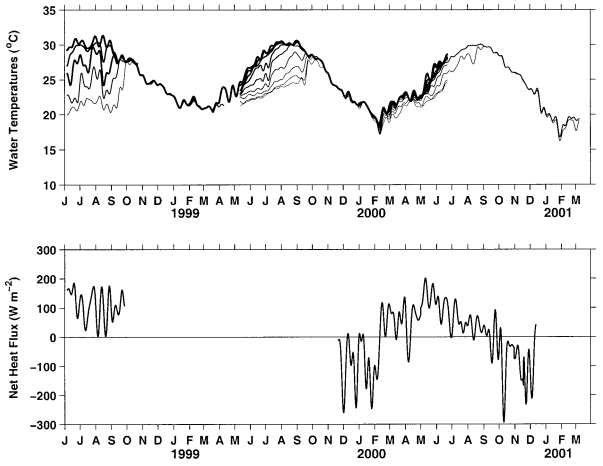

FIG. 8. WFS measurements from Jun 1998 to Mar 2001. (top) The 10-day low-pass-filtered CM2 water temperatures at 1-, 5-, 10-, 15-, 20-, 25-, 30-, 35-, and 40-m depths. The line thickness thins with increasing depth: the thickest is at 1 m; the thinnest is at 40 m. (bottom) The 10-day low-pass-filtered net heat flux calculated from measured parameters. Data from all three moorings are combined to get the net heat flux series.

surface heat flux from positive to negative. The largest depth-averaged temperature increase (3.86°C) is during May; 61% of this is due to the surface heat flux (2.35°C) and the other 39% is due to ocean dynamics (1.51°C). Although heat flux is the largest contributor to temperature change during May, ocean dynamics are responsible for the synoptic-scale variability (shown in Fig. 9b and obtained from the standard deviation). The relative influences of surface heat flux and ocean dynamics are almost equal in June, which has a total vertically integrated temperature increase of 2.32°C. In this case, the ocean dynamics account for 55.5% (1.31°C), and the heat flux accounts for 43.5% (1.01°C). The daily mean net heat flux begins to change sign from positive to negative during June. This is evident in July when the surface heat flux has a cooling effect (−0.08°C) and ocean dynamics (0.81°C) are mostly responsible for the change in the vertically averaged temperatures (0.74°C). No upwelling events are observed in July and the only downwelling event observed serves to destratify and increase the overall water column temperature, thereby increasing the vertically averaged temperature. Contrary to May, the synoptic-scale variability during July was mostly in response to variations in the surface heat flux.

The relative influences of heat flux and ocean circulation dynamics on the spring transition period were also investigated by He and Weisberg (2002b) using a regional adaptation of the Princeton Ocean Model forced by NCEP reanalysis wind and heat flux, and by river inflows. Consistent with our results from May 2000, they found that heat flux largely controls the spring season transition of water temperature. Large synoptic-scale variations were attributed to a combination of ocean circulation dynamics and surface heat flux. With shoaling water depth, the convergence of heat flux by the ocean circulation plays a proportionately larger role.

Annual cooling and destratification of the water column begins almost concurrently at all locations during September of each year, and continues throughout the fall and winter. The daily mean surface heat flux continues to decrease and becomes almost entirely negative as the cooling continues. During September and October 2000 (Fig. 10), the mean vertically integrated temperature changes by −4.72°C. Over this period, ocean dynamics continues to have a marginal warming effect (0.51°C), but the major factor in the observed heat loss is due to the surface heat flux (−5.23°C). Analogous with the spring season transition, the heat flux largely controls the fall season transition of water temperature change, but the ocean dynamics are mainly responsible for the synoptic-scale variability.

The cooling of the water column is not gradual during the fall transition period. Instead it occurs in a series of steplike decreases in temperature at all depths (Fig. 10a). This is the peak of the hurricane season and some of the observed decreases in water temperature are due to the passage of tropical storms or hurricanes. Hurricane Gordon, 16–19 September 2000, for example, results in a maximum daily net heat loss of almost −300 W m^{-2}, and a depth-average temperature change of −0.75°C at NA2 (Fig. 10a). The surface heat flux accounts for 80% of this decrease (−0.6°C) and ocean circulation is responsible for the other 20% (−0.15°C). The fall cooling and destratification begins in earnest once the first major tropical storm passes by. The high winds lead to a well-mixed water column (even at CM2, which is twice as deep as NA2). The temperature decrease during the tropical storm, and the generally negative net heat flux dur-

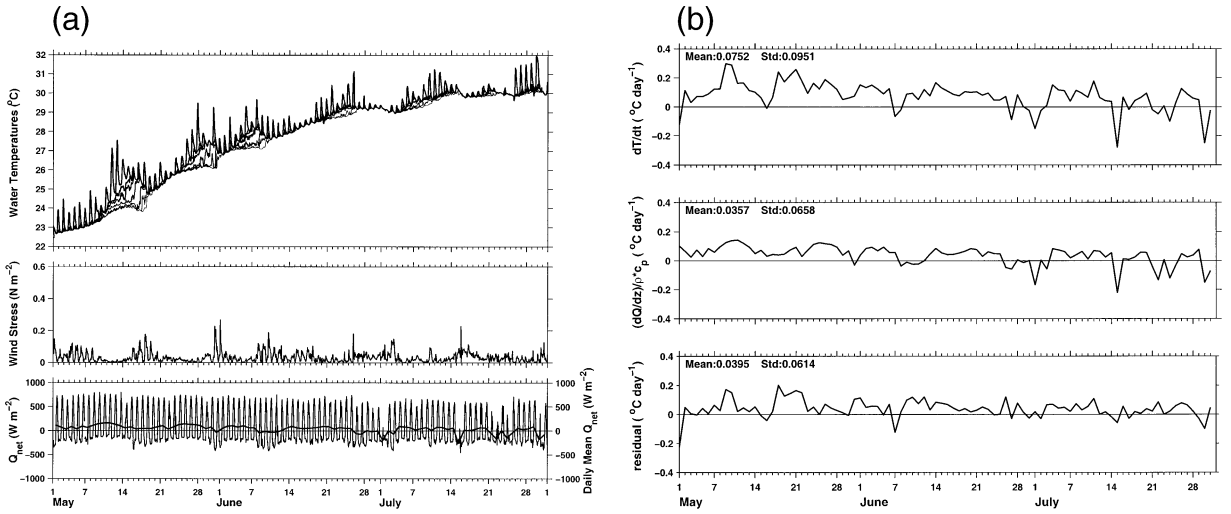

FIG. 9. (a) Top panel shows hourly averaged NA2 water temperatures from May to Jul 2000 at 1-, 4-, 7-, 10-, 13-, 16-, and 19-m depths. The line thickness thins with increasing depth. Middle panel shows hourly averaged wind stress. Bottom panel shows the net heat flux (thin line) and its daily mean (thick line). (b) Components of the one-dimensional temperature equation from May to Jul 2000 at NA2. Top panel shows depth-averaged temperature change; middle panel shows surface heat flux; bottom panel shows the residual, which combines ocean dynamics and errors.

ing this time of year ensures that water temperatures cannot warm up again following a storm. Therefore the water continues to cool and the water column remains destratified.

We need to be cautious in attributing all the steplike decreases in temperature to tropical storms during this season. Extratropical weather systems are also very important. For example, the temperature decreases by ~3°C between 9 and 15 October 2000 (Fig. 10a). This decrease coincides with an increase in wind speed and barometric pressure, a decrease in air temperature and relative humidity, an increase in the net longwave radiation loss from the ocean, and unusually large increases in both latent and sensible heat losses (Fig. 11), resulting in an increase in the net heat loss (Fig. 10a). The latent and sensible heat losses are partially a result of the increased wind speed, but that alone cannot account for the large variation. Air temperature decreases by 7° from ~25°C to a minimum of 18°C, which also increases the sensible heat flux. Relative humidity decreases substantially from about 78% to less than 60%, which contributes to the increase in the latent heat flux. These observations suggest that the passing of an extratropical front over this region, with a drier, cooler air mass, results in increased evaporation and cooling, which in turn results in cooler SSTs. Some of these

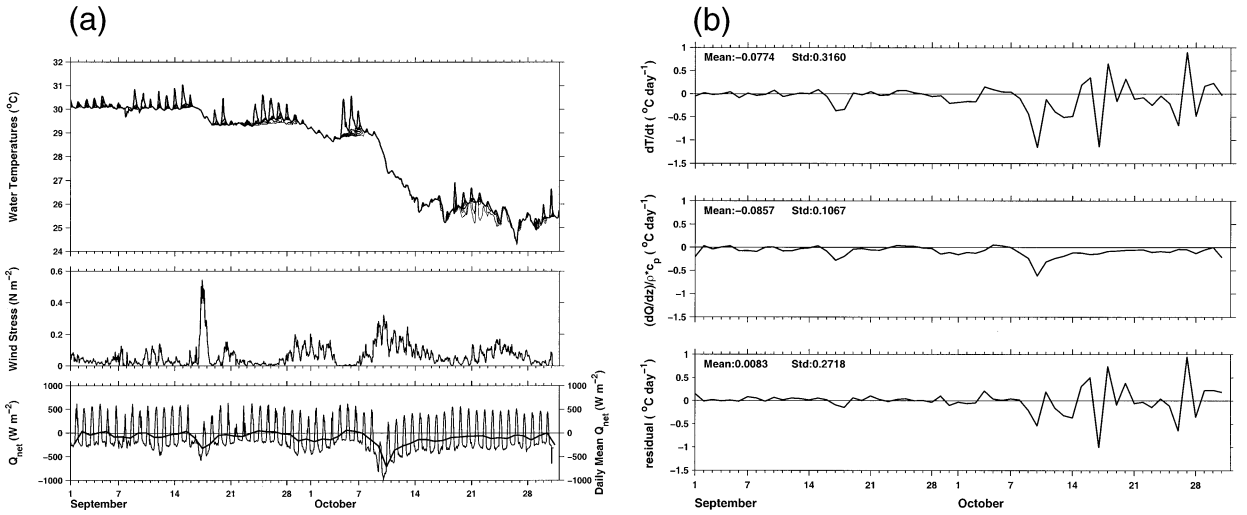

FIG. 10. (a) Same as for Fig. 9a, but during Sep–Oct 2000. Hurricane Gordon passed the mooring between 16 and 19 Sep. An extratropical weather system with cool, dry air passed the mooring between 9 and 15 Oct. (b) Same as for Fig. 9b, but during Sep–Oct 2000.

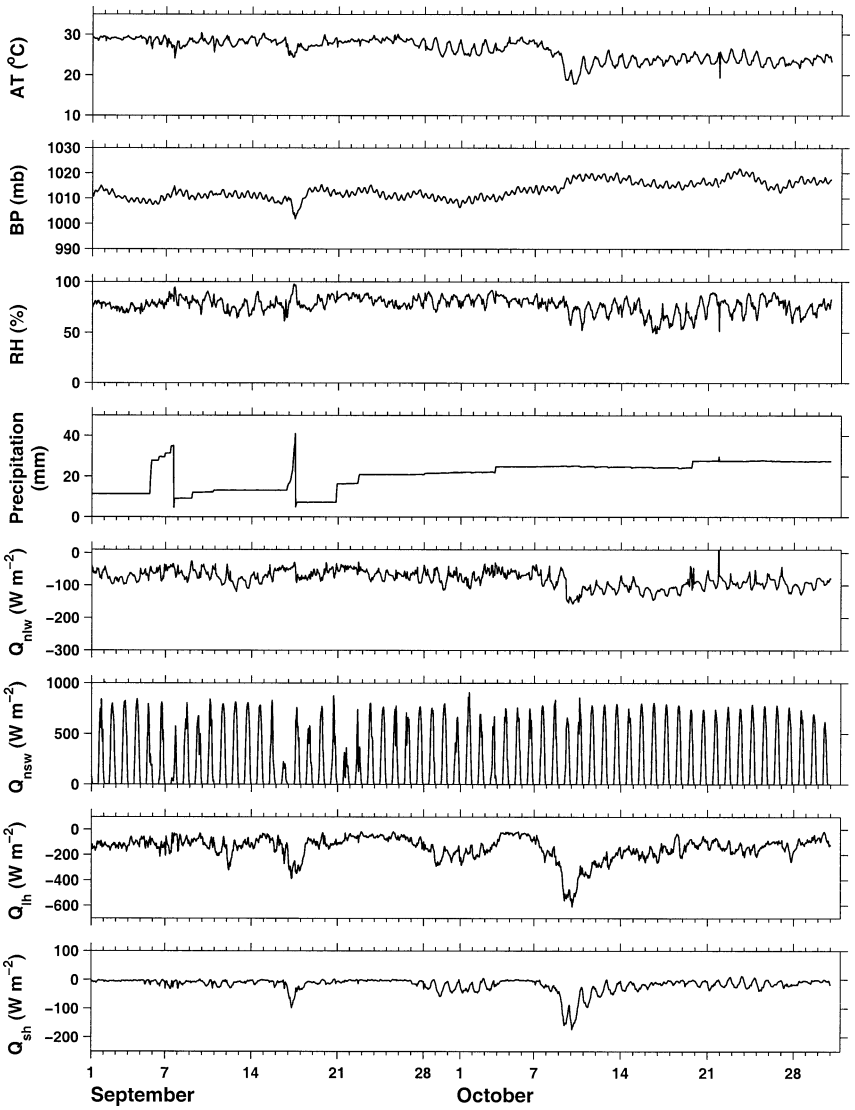

FIG. 11. Hourly averaged time series of measured meteorological variables and calculated heat fluxes from NA2 for Sep and Oct 2000.

sudden decreases in water temperature are accompanied by a rapid loss of heat from the ocean, so for example, during this October event the net surface heat flux approached -1000 W m^{-2}. Heat flux in this case accounts for 69% of the large temperature cooling during the event; ocean dynamics accounts for the other 31%. We see that tropical storms do not necessarily have the largest impact on WFS ocean–atmosphere fluxes.

There are other large changes in the vertically averaged temperature during October, especially around the 17th and 27th, which cannot be accounted for by passing storms or large heat flux changes, but are a consequence of ocean dynamics. Observations show that, following periods of sustained northerly winds, strong southward subsurface currents advect cooler water into the region from the north.

The influence of ocean dynamics and heat flux on the depth-averaged temperature change differs during September and October. In September, the temperature cools by -0.96°C as a result of surface cooling (-1.52°C) offset by ocean dynamical warming (0.56°C). In October however, the combined cooling effects due to net heat flux (-3.71°C) and ocean dynamics (-0.06°C) lead to a temperature change of -3.76°C. Constructive and destructive interference between ocean circulation and surface heat flux influences on temperature can either accentuate or mitigate water column temperature changes.

The minimum temperature is usually in February of each year, except during 1999 when a warming of the water column at all locations occurred from mid-January to mid-February. This reversed the normal cooling trend and ensured that temperatures did not get as cold as in other years; at CM2 they remained above 20°C

(Fig. 8). This warming was partly attributable to very low wind speeds that resulted in smaller latent and sensible heat losses. The latent heat flux was close to zero for most of this time. This was also accompanied by extraordinarily high relative humidity, reaching supersaturation (maximum values of 3%) at NA2 and almost 100% relative humidity at CM2 for a few days in both January and February. Although there are no in situ measurements of precipitation available, the salinity showed a large decrease ($>$1.5 psu) at the surface during this time, coinciding with a period of heavy rainfall as seen in the Huffman et al. (2001) Global Preciption Climatology Project's (GPCP's) One-Degree Daily Precipitation Data Set. The coldest temperatures in 1998 at NA2 (minimum of 18°C) were in January, whereas at EC3 (minimum of 20°C) they were in March, showing that even though the moorings were only 8.8 km apart, water temperature variations exist on that scale.

These data also reveal an interannual variability in ocean temperatures: the wintertime temperatures got increasingly colder from 1998 to 2000. In 1998, at CM2 the subsurface temperatures were cooler, but the surface temperatures were warmer ($>$28.5°C) for a longer period of time than in subsequent years or at other locations. The CM2 data also showed interannual variability in the stratification, which decreased in magnitude and temporal extent from 1998 to 2000.

5. Conclusions

In situ measurements of oceanic and atmospheric variables from the west Florida shelf from 1998 to 2001 are used to describe features of the annual cycle of SST and heat flux. Generally, when the heat flux switches sign from negative to positive, SST is at its minimum and the water column begins to warm up, and conversely, when the heat flux switches sign from positive to negative.

Observations during the spring season transition show a series of synoptic-scale momentum and heat flux variations that result in stratification of the water column. These synoptic variations are most evident in shallow water where smaller fluxes are required to affect change. Model studies show similar behaviors (He and Weisberg 2002b).

Analyses of the one-dimensional temperature equation show how the relative importance between surface heat flux and ocean dynamics changes seasonally in controlling the water temperature. Observations from the end of the spring 2000 transition season show that the depth-averaged temperature change is predominantly due to surface heat flux, and the synoptic-scale variability is primarily by ocean dynamics. During summer, this situation is reversed and the major influence on the depth-averaged temperature is ocean dynamics, with heat flux being responsible for the synoptic variability. Water temperature increases due to advection of warm water from the south, but is partially offset by synoptic-scale ocean cooling events when the net surface heat flux changes from positive to negative.

Cooling and destratification of the water column characterizes the fall season. This occurs as a series of steplike decreases in the water temperature. Some of these are attributable to tropical storms, but others are a consequence of surface heat flux change due to extratropical fronts, or ocean dynamics as cool water is advected into the region. The passage of the first tropical storm of the season heralds the subsequent decline in water temperature: the storm-induced temperature decrease coupled with the generally negative net heat flux during this time ensures that the water column cannot warm up again. Although the largest momentum flux is associated with tropical storms, they do not necessarily have the largest impact on ocean–atmosphere heat fluxes. The largest observed change in surface heat flux (and water temperature decrease) on the WFS was in response to an extratropical weather system. As in spring, surface heat flux is the predominant driver of the fall water temperature transition, and synoptic-scale variability is primarily due to ocean circulation dynamics.

There is also evidence of interannual variability: the wintertime temperatures got increasingly colder from 1998 to 2000, and the stratification was greatest and the subsurface temperatures were coldest in 1998 when compared to subsequent years. There was also an unusual warming in early 1999, which prevented the water temperatures from getting as cold as observed in other years. The data suggest that this was due to low winds and minimal latent heat loss.

Heat fluxes from different climatologies differ greatly. The NCEP fields are useful in providing a large-scale picture, but they are unable to reproduce important regions of spatial flux variability shown by in situ and satellite measurements. Driving ocean models with the reanalysis fields, without flux corrections, fails to produce observed seasonally varying features on the WFS. Reconciling these differences and their impacts on regional climate variability studies provides challenges to coupled ocean–atmosphere models and their supporting observing systems.

Acknowledgments. This work was supported by the Office of Naval Research (Grant N00014-98-1-0158) and the National Oceanic and Atmospheric Administration, (Grant NA76RG0463). Special thanks are offered to the family of Elsie and William Knight for the fellowship endowment that helped to support J. I. Virmani. Field work and computing support was provided by Ocean Circulation Group members: Messrs. R. Cole, J. Donovan, C. Merz, and P. Smith, and discussions with R. He, R. Helber, and Y. Liu proved helpful. Mooring work was conducted with the help of the crew of the *R/V Suncoaster*. NCEP reanalysis data were obtained from the NOAA-CIRES Climate Diagnostics Center, Boulder, CO (http://www.cdc.noaa.gov/). The authors

would like to thank the reviewers for their constructive comments.

REFERENCES

Anderson, E. R., 1952: Energy budget studies, water-loss investigations: Lake Hefner studies. *U.S. Geol. Surv. Circ.,* **229,** 71–88.

Berliand, M. E., and T. G. Berliand, 1952: Measurements of the effective radiation of the Earth with varying cloud amounts (in Russian). *Izv. Akad. Nauk SSSR, Ser. Geofiz.,* **1,** 64–78.

Blaha, J., and W. Sturges, 1981: Evidence for wind-forcing circulation in the Gulf of Mexico. *J. Mar. Res.,* **39,** 711–733.

Bunker, A. F., 1976: Computations of surface energy flux and annual air–sea interaction cycles of the North Atlantic Ocean. *Mon. Wea. Rev.,* **104,** 1122–1140.

Clark, N. E., L. Eber, R. M. Laurs, J. A. Renner, and J. F. T. Saur, 1974: Heat exchange between ocean and atmosphere in the eastern North Pacific for 1961–1971. NOAA Tech. Rep. NMFS SSRF-682, NOAA, 108 pp.

Clarke, A. J., and K. H. Brink, 1985: The response of stratified, frictional flow of shelf and slope waters to fluctuating large-scale low frequency wind forcing. *J. Phys. Oceanogr.,* **15,** 439–453.

Cragg, J., G. Mitchum, and W. Sturges, 1983: Wind-induced sea-surface slopes on the West Florida Shelf. *J. Phys. Oceanogr.,* **13,** 2201–2212.

Da Silva, A. M., C. C. Young, and S. Levitus, 1994: *Algorithms and Procedures.* Vol. 1, *Atlas of Surface Marine Data 1994,* NOAA Atlas NESDIS 6, 83 pp.

Fernandez-Partagas, J., and C. N. K. Mooers, 1975: A subsynoptic study of winter cold fronts in Florida. *Mon. Wea. Rev.,* **103,** 742–744.

He, R., and R. H. Weisberg, 2002a: Tides on the West Florida Shelf. *J. Phys. Oceanogr.,* **32,** 3455–3473.

——, and ——, 2002b: West Florida Shelf circulation and temperature budget for the 1999 spring transition. *Cont. Shelf Res.,* **22,** 719–748.

Hellerman, S., and M. Rosenstein, 1983: Normal monthly wind stress over the world ocean with error estimates. *J. Phys. Oceanogr.,* **13,** 1093–1104.

Huffman, G. J., R. F. Adler, M. Morrissey, D. T. Bolvin, S. Curtis, R. Joyce, B. McGavock, and J. Susskind, 2001: Global precipitation at one-degree daily resolution from multi-satellite observations. *J. Hydrometeor.,* **2,** 36–50.

Huh, O. K., W. J. Wiseman Jr., and L. J. Rouse Jr., 1981: Intrusion of loop current waters onto the West Florida Continental Shelf. *J. Geophys. Res.,* **86,** 4186–4192.

Jerlov, N. G., 1968: *Optical Oceanography.* Elsevier, 199 pp.

Josey, S. A., D. Oakley, and R. W. Pascal, 1997: On estimating the atmospheric longwave flux at the ocean surface from ship meteorological reports. *J. Geophys. Res.,* **102,** 27 961–27 972.

Koblinsky, C. J., 1981: The M_2 tide on the West Florida Shelf. *Deep-Sea Res.,* **28A,** 1517–1532.

Marmorino, G. O., 1982: Wind-forced sea level variability along the West Florida Shelf. *J. Phys. Oceanogr.,* **12,** 389–404.

——, 1983: Variability of current, temperature, and bottom pressure across the West Florida Continental Shelf, winter 1981–1982. *J. Geophys. Res.,* **88,** 4439–4457.

Maul, G., 1977: The annual cyclone of the Gulf Loop Current. Part I: Observations during a one year time series. *J. Mar. Res.,* **35,** 29–47.

Meyers, S. D., E. M. Siegel, and R. H. Weisberg, 2001: Observations of currents on the West Florida Shelf break. *Geophys. Res. Lett.,* **28,** 2037–2040.

Mitchum, G. T., and W. Sturges, 1982: Wind-driven currents on the West Florida Shelf. *J. Phys. Oceanogr.,* **12,** 1310–1317.

——, and A. J. Clarke, 1986: The frictional nearshore response to forcing by synoptic scale winds. *J. Phys. Oceanogr.,* **16,** 934–946.

Niiler, P. P., 1976: Observations of low-frequency currents on the West Florida Continental Shelf. *Mem. Soc. Roy. Sci. Leige,* **6,** 331–358.

Paulson, C. A., and J. J. Simpson, 1977: Irradiance measurements in the upper ocean. *J. Phys. Oceanogr.,* **7,** 952–956.

Price, J. F., C. N. K. Mooers, and J. C. van Leer, 1978: Observation and simulation of storm-induced mixed-layer deepening. *J. Phys. Oceanogr.,* **8,** 582–599.

Rasmusson, E. M., 1967: Atmospheric water vapor transport and the water balance of North America: Part I. Characteristics of the water vapor flux field. *Mon. Wea. Rev.,* **95,** 403–426.

Sturges, W., 1994: The frequency of ring separations from the loop current. *J. Phys. Oceanogr.,* **24,** 1647–1651.

——, and R. Leben, 2000: Frequency of ring separations from the loop current in the Gulf of Mexico: A revised estimate. *J. Phys. Oceanogr.,* **30,** 1814–1819.

Vukovich, F. M., 1988: Loop current boundary variations. *J. Geophys. Res.,* **93,** 15 585–15 591.

Wang, C., and D. Enfield, 2001: The tropical Western Hemisphere Warm Pool. *Geophys. Res. Lett.,* **28,** 1635–1638.

Weatherly, G. L., and D. Thistle, 1997: On the wintertime currents in the Florida Big Bend Region. *Cont. Shelf Res.,* **17,** 1297–1319.

Weisberg, R. H., 1996: On the evolution of SST over the PACS region. Preprints, *Eighth Conf. on Air–Sea Interaction,* Atlanta, GA, Amer. Meteor. Soc., p. 378.

——, B. D. Black, and H. Yang, 1996: Seasonal modulation of the West Florida Continental Shelf circulation. *Geophys. Res. Lett.,* **23,** 2247–2250.

——, ——, and Z. Li, 2000: An upwelling case study on the Florida's West Coast. *J. Geophys. Res.,* **105,** 11 459–11 469.

——, Z. Li, and F. E. Muller-Karger, 2001: West Florida Shelf response to local wind forcing: April 1998. *J. Geophys. Res.,* **106,** 31 239–31 262.

Weller, R. A., and S. Anderson, 1996: Surface meteorology and air–sea fluxes in the western equatorial Pacific warm pool during the TOGA Coupled Ocean–Atmosphere Response Experiment. *J. Climate,* **9,** 1959–1990.

Williams, J., W. F. Grey, E. B. Murphy, and J. J. Crane, 1977: Memoirs of the Hourglass Cruises, Rep. IV(III). Marine Research Laboratory, Dept. of Natural Resources Contribution Number 300, St. Petersburg, FL, 134 pp.

Yang, H., and R. H. Weisberg, 1999: Response of the West Florida Shelf circulation to climatological wind stress forcing. *J. Geophys. Res.,* **104,** 5301–5320.